HHS Public Access

Author manuscript

Mol Microbiol. Author manuscript; available in PMC 2018 April 01.

Published in final edited form as:

Mol Microbiol. 2017 April ; 104(2): 334–348. doi:10.1111/mmi.13630.

Perturbation of manganese metabolism disrupts cell division in *Streptococcus pneumoniae*

Julia E. Martin[a], **John P. Lisher**[a,b], **Malcolm E. Winkler**[c,d], and **David P. Giedroc**[a,d,#]

[a]Department of Chemistry, Indiana University, Bloomington, IN, 47405-7102, USA

[b]Graduate Program in Biochemistry, Indiana University, Bloomington, IN, 47405, USA

[c]Department of Biology, Indiana University, Bloomington, IN, 47405, USA

[d]Department of Molecular and Cellular Biochemistry, Indiana University, Bloomington, IN, 47405, USA

Abstract

Manganese (Mn) is an essential micronutrient and required cofactor in bacteria. Despite its importance, excess Mn can impair bacterial growth, the mechanism of which remains largely unexplored. Here, we show that proper Mn homeostasis is critical for cellular growth of the major human respiratory pathogen *Streptococcus pneumoniae*. Perturbations in Mn homeostasis genes, *psaBCA,* encoding the Mn importer, and *mntE*, encoding the Mn exporter, lead to Mn sensitivity during aerobiosis. Mn-stressed cells accumulate iron and copper, in addition to Mn. Impaired growth is a direct result of Mn toxicity and does not result from iron-mediated Fenton chemistry, since cells remain sensitive to Mn during anaerobiosis or when hydrogen peroxide biogenesis is significantly reduced. Mn-stressed cells are significantly elongated, whereas Mn-limitation imposed by zinc addition leads to cell shortening. We show that Mn accumulation promotes aberrant dephosphorylation of cell division proteins via hyperactivation of the Mn-dependent protein phosphatase PhpP, a key enzyme involved in the regulation of cell division. We discuss a mechanism by which cellular Mn:Zn ratios dictate PhpP specific activity thereby regulating pneumococcal cell division. We propose that Mn-metalloenzymes are particularly susceptible to hyperactivation or mismetallation, suggesting the need for exquisite cellular control of Mn-dependent metabolic processes.

Graphical abstract

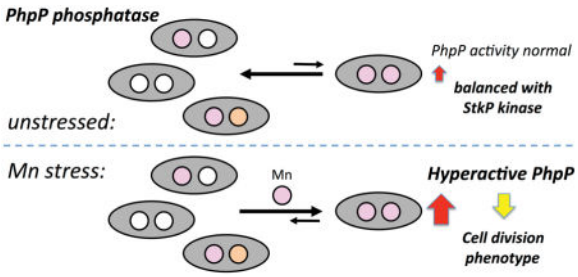

[#]Corresponding author: (812) 856-3178; fax (812) 856-5710; giedroc@indiana.edu.

INTRODUCTION

Bacteria maintain transition metal quota and homeostasis by deploying high-affinity, metal-specific transporters that scavenge metal from diverse microenvironments and efflux excess metal from the cytoplasm. Iron (Fe) and zinc (Zn) systems are the most extensively studied and best understood. However, there is increasing interest in manganese (Mn) because of its necessity during conditions of host-generated oxidative stress and in facilitating virulence of numerous pathogenic bacteria (Kelliher and Kehl-Fie, 2016; German *et al.*, 2016), including *Streptococcus pneumoniae* (Marra *et al.*, 2002; Rosch *et al.*, 2009; van Opijnen *et al.*, 2009).

In *S. pneumoniae*, Mn homeostasis is governed by expression and activities of two metal transporters, the sole Mn-specific importer PsaBCA (Marra *et al.*, 2002) and the constitutively expressed cation diffusion facilitator (CDF) family exporter MntE (Rosch *et al.*, 2009; Martin and Giedroc, 2016). Intracellular bioavailable Mn is sensed by PsaR, a homodimeric MntR/DtxR family repressor (Higgins and Giedroc, 2013) that binds two pairs of metals per dimer to form a Mn_2Zn_2 mixed metal or Mn_4:PsaR complex (Lisher *et al.*, 2013). During Mn-replete growth, the regulatory Mn site in PsaR recruits D7 from the N-terminal α-helix into the Mn(II) chelate, thereby allosterically activating DNA binding, leading to repression of *psaBCA* transcription and decreased Mn import (Lisher *et al.*, 2013). In liquid culture, *S. pneumoniae* fails to grow aerobically in the absence of Mn and cells lacking *mntE* are extremely sensitive to Mn toxicity (Rosch *et al.*, 2009; Dintilhac *et al.*, 1997). Both the PsaBCA importer and the MntE exporter are important for the virulence of *S. pneumoniae* (Rosch *et al.*, 2009; Marra *et al.*, 2002; van Opijnen *et al.*, 2009) and PsaBCA is important for colonization (van Opijnen *et al.*, 2009), suggesting that management of bioavailable Mn is critical for pneumococcal survival during pathogenesis.

The specific functional roles for which Mn is required, however, are not fully characterized. For many bacteria, Mn serves as a substitute for Fe in non-heme, mononuclear Fe metalloenzymes when Fe is scarce or vulnerable to Fenton chemistry (the oxidation of Fe by hydrogen peroxide (H_2O_2)) (Imlay, 2014; Lisher and Giedroc, 2013). However, recent evidence suggests that the functional roles of intracellular Mn may be more extensive, with potential impact on carbon metabolism, phosphorylation and signaling, cyclic-di-GMP synthesis, and hydrolysis (Papp-Wallace and Maguire, 2006). To date, there are seven known Mn-requiring enzymes expressed by *S. pneumoniae*. These include the sole superoxide dismutase SodA used to detoxify superoxide anion; the sole aerobic ribonucleotide reductase NrdEF for the *de novo* synthesis of deoxyribonucleotides required for DNA replication and repair; the inorganic pyrophosphatase PpaC for phosphorus metabolism; the phosphopentomutases Pgm and DeoB which connect glycolysis to polysaccharide capsule biosynthesis and the pentose phosphate pathway to purine biosynthesis, respectively; the tyrosine protein phosphatase CpsB which regulates polysaccharide capsule formation; and the sole serine/threonine protein phosphatase PhpP, a key protein involved in regulating cell division (Lisher *et al.*, 2013; Li *et al.*, 2014; Rosch *et al.*, 2009; Yesilkaya *et al.*, 2000; Novakova *et al.*, 2005; Morona *et al.*, 2002; Panosian *et al.*, 2011).

Accumulating evidence indicates that Mn homeostasis is interconnected with both Fe and Zn homeostasis in bacteria (Eijkelkamp *et al.*, 2014; Imlay, 2014; Honsa *et al.*, 2013; Jacobsen

et al., 2011). In *S. pneumoniae*, excess Zn is capable of imposing Mn limitation by binding the high-affinity Mn solute-binding protein PsaA of the PsaBCA Mn-importer, forming a stable Zn-protein complex that prohibits Zn release, rendering the PsaBCA importer nonfunctional (Counago *et al.*, 2014). Severe Mn limitation in return can induce *czcD* transcription (encoding the Zn CDF effluxer), thereby reducing cell associated Zn concentration (Ogunniyi *et al.*, 2010). In *Escherichia coli*, excess Mn can disrupt Fe homeostasis by activating the ferric uptake regulator, Fur, with the resultant intracellular high Mn:Fe ratio capable of blocking heme biosynthesis (Martin *et al.*, 2015). In other bacteria, Mn levels can influence the activation of the Fe-regulatory peroxide sensor protein PerR (Fuangthong *et al.*, 2002; Helmann, 2014; Wu *et al.*, 2006; Morrissey *et al.*, 2004). The absence of significant numbers of [4Fe-4S]- and heme-containing enzymes, as well as Fur and PerR in the Mn-centric pathogen *S. pneumoniae* suggests that the mechanism of Mn-mediated toxicity may be distinct from that of *E. coli* and other Fe-centric bacteria, where the intracellular Mn:Fe ratio is ≤0.1 (Lisher and Giedroc, 2013). We propose here that Mn-requiring enzymes, in harboring a cofactor that binds most weakly to proteins among other first row, late *d*-block transition metals, are metallated by default, and are therefore particularly prone to mismetallation or over-metallation, with the identity of the bound metal strongly influenced by the intracellular bioavailable pool of metals (Tottey *et al.*, 2008).

RESULTS

Manganese homeostasis is critical for cell growth

To investigate the mechanism of Mn toxicity in *S. pneumoniae* D39, we constructed strains harboring deletion or missense alleles of *psaR*, encoding the Mn-specific regulator, and *mntE,* encoding the Mn-specific CDF effluxer, singly or in combination, and assessed physiological changes in the presence and absence of Mn added to cultures. We find here that *psaR*-null mutants mimic wild-type (WT) growth and are insensitive to increasing Mn concentrations (Fig. 1A–C and S1); further, cell-associated Mn levels are also WT-like (Fig. S2A), with only moderately more Mn associated with *psaR* mutants versus WT cells. The lack of Mn sensitivity for *psaR*-null mutants is consistent with the fact that MntE is constitutively expressed in *S. pneumoniae* (Martin and Giedroc, 2016; Rosch *et al.*, 2009). This contrasts sharply with *Bacillus subtilis* where strains lacking the Mn-specific regulator MntR are highly sensitive to Mn toxicity (Fisher *et al.*, 1973). Unlike *S. pneumoniae*, MntR is required for induction of Mn efflux in response to Mn stress for *B. subtilis* (Huang *et al.*, 2017).

Consistent with previous reports (Rosch *et al.*, 2009; Martin and Giedroc, 2016), *S. pneumoniae mntE*-null mutants are sensitive to increasing Mn concentrations (Fig. 1A–C and S1) and ICP-MS shows ≥2-fold increase in cell-associated Mn compared to WT cells during Mn-toxicity (Fig. S2A). At 200 μM Mn, *mntE*-null mutants double several times before entering a growth arrested phase that lasts for several hours after which growth recovery begins (Fig. 1B). This growth arrest is reminiscent of that observed by Mn stress in *E. coli* and in *B. subtilis* (Martin *et al.*, 2015; Fisher *et al.*, 1973). Complementation of *mntE* in the pneumococcus restores growth to WT-levels during Mn toxicity (Fig. 1D, Fig. S1F).

In contrast to WT and single mutant strains, the double *psaR*- and *mntE*-null mutant strain is highly sensitive to Mn (Fig. 1A–C and S1); its growth is significantly diminished in unsupplemented BHI broth (Fig. 1A), which contains only ≈20 nM Mn as prepared. Nearly 10-fold more Mn accumulates in the *psaR mntE* mutants compared to WT unstressed cells (Fig. S2). We also tested the effect of Mn toxicity on a pneumococcal strain expressing a crippled PsaR , *e.g.,* a mutant PsaR-(D7A) that retains one metal-binding site but poorly represses transcription of *psaBCA* (Lisher *et al.*, 2013); PsaR-(D7A) expressed from its native locus in the *mntE* background provides some protection against Mn toxicity relative to *psaR mntE* mutants, but only at lower Mn concentrations (≤50 μM) (Fig. 1C). Together, these data suggest that regulation of Mn homeostasis is critical for survival of *S. pneumoniae*, and that both the Mn effluxer MntE and the Mn importer PsaBCA function collaboratively to maintain optimal intracellular Mn bioavailability.

Manganese stress affects homeostasis of other transition metals

We next investigated the impact of Mn perturbation on the homeostasis of other transition metals using ICP-MS. We find that deletion of *mntE* does not alter metal homeostasis of Mn, Fe, Zn and Cu during routine unstressed growth (Fig. 1E, *darker* shaded bars). However, during Mn-stress *mntE*-null mutants accumulate 3.5-fold and 3-fold more Fe and Cu, respectively, relative to WT Mn-stressed cells after 3.5 h, within the growth arrested phase (Fig. 1E; see Fig. 1B). Zn levels also surprisingly increased 2-fold in the *mntE*-null mutant when stressed with Mn relative to WT and *mntE* unstressed strains. At 7 h, when *mntE*-null mutants exit the growth arrested phase, the Fe level falls dramatically while Zn and Cu are relatively unaltered (Fig. 1F) relative to *mntE* samples measured at 3.5 h (Fig. 1E). Transcriptional analysis at 3.5 h growth reveals that Fe-acquisition genes, *pitA* (Rosch *et al.*, 2009) and *piuB*, are upregulated by Mn stress, whereas *piaB* is unaffected (Fig. 1G), consistent with elevated Fe in these cells during the growth arrested phase (Fig. 1E, *red* bars). Transcription of the gene encoding the orphan response regulator, *ritR*, is also induced, more so in the *mntE* strain (Fig. 1G). Although RitR represses transcription of *piu* and *pia* (Ulijasz *et al.*, 2004; Honsa *et al.*, 2013), its response trigger for DNA binding is unknown since it lacks the key Asp residue involved in the phosphoryl signal relay process (Maule *et al.*, 2015). Mn-stressed *mntE* mutants also induced *copA* transcription (Fig. 1G), consistent with an accumulation of Cu observed by ICP-MS (Fig. 1E, *blue* bars). Although the mechanism is unclear, these data show that misregulation of Mn homeostasis impacts the homeostasis of other transition metals.

Experiments were next carried out to identify what cellular processes might be affected by misregulation of Mn homeostasis. *S. pneumoniae* is a lactic acid bacterium that endogenously synthesizes H_2O_2 as a byproduct of the activities of pyruvate oxidase (SpxB) and lactate oxidase (LctO) during aerobic growth (Pericone *et al.*, 2003; Ramos-Montanez *et al.*, 2008; Echlin *et al.*, 2016) (Fig. S3A). In other bacteria such as *E. coli*, high concentrations of Fe and Cu decrease cell growth in the presence of exogenous H_2O_2 by damaging biomolecules via Fenton chemistry, and through mismetallation of metalloproteins, respectively (Imlay, 2014). However, chelation of Fe and Cu using Fe- and Cu-specific chelators, desferrioxamine (DFO) and bicinchoninic acid (BCA) (Lisher *et al.*, 2017; Fu *et al.*, 2013), respectively, fail to protect cells from Mn toxicity (Fig. S4).

A previous report that characterized *mntE* in the pneumococcal strain TIGR4 serotype 4 showed that Mn stress increases H_2O_2 production on solid medium (Rosch *et al.*, 2009). However, we find that in serotype 2 pneumococcal strain D39, Mn-stressed *mntE* mutants produce slightly less H_2O_2 than wild-type cells when grown in liquid broth (Fig. S3B). This decrease cannot be attributed to slow growth of *mntE*, a block in glycolysis, or inhibition of SpxB activity via mismetallation (Fig. S3C–E). In addition, supplementation with catalase has little effect on the growth arrest and *mntE* mutants lacking *spxB* and *lctO*, which together contribute ≈98% of the endogenous H_2O_2 in *S. pneumoniae* (Lisher *et al.*, 2017), grow similarly to *mntE* single mutants during Mn-stress (Fig. S3F–G). Cellular Mn sensitivity is also observed during anaerobic growth (Fig. 2A–B), while both WT and *mntE*-null mutants accumulate significant Mn relative to unstressed cells (Fig. 2C). In contrast to aerobically grown cells, Zn and Cu levels are not significantly altered and Fe levels are actually reduced 3-fold by Mn treatment in both WT and *mntE* mutant cells (Fig. 2C). These findings collectively suggest that oxidative stress, linked, for example, to misregulation of cellular Fe levels, is not a major factor in the pronounced Mn-mediated growth phenotype in *mntE* mutants.

Cell division is disrupted in manganese-stressed cells

We next assessed cell morphology. Encapsulated *S. pneumoniae* D39 typically forms short chains or pairs (diploid) of ellipsoidal cells, even in the presence of Mn (Fig. 3A) (Barendt *et al.*, 2009). Cells lacking *psaR* are only slightly perturbed, displaying generally longer chains with few elongated cells. Severe morphological changes are observed in *mntE* mutants. The majority of *mntE* mutant cells were elongated (Fig. 3A–C), with some cells enlarged (rounded) and apparently undergoing asymmetric cell division (Fig. 3A). Residual lysed cells are also observed. Similar defects in cell morphologies were observed in the *psaR mntE* double mutant strain, which additionally forms exceedingly long chains of cells. Pronounced cell elongation is also observed during anaerobic growth with Mn (Fig. 3D–E). In contrast to Mn toxicity, Mn limitation imposed by zinc toxicity (Jacobsen *et al.*, 2011; Eijkelkamp *et al.*, 2014) (Fig. S5) leads to dramatically shortened cells (Fig. 3B–C). These findings suggest that perturbations in the regulation of cell division could be responsible for these striking effects on cell morphology.

To test this idea, we focused on the obligate Mn-requiring eukaryotic-like PP2C Ser/Thr phosphatase PhpP (Dworkin, 2015; Novakova *et al.*, 2005), which is one half of the eukaryotic-like Ser/Thr kinase (StkP)-phosphatase pair known to impact cell division in *S. pneumoniae* (Fig. S6A). StkP and PhpP are functionally coupled and physically interact to regulate the activities of a handful of proteins by dynamically controlling the net phosphorylation status on Ser/Thr residues (Fig. S6A) (Beilharz *et al.*, 2012; Fleurie *et al.*, 2014a; Novakova *et al.*, 2010). DivIVA and MapZ are two proteins involved in cell division and whose functions are regulated by phosphorylation via StkP/PhpP (Massidda *et al.*, 2013; Fleurie *et al.*, 2014a). We find a statistically significant decrease in Thr-phosphorylation of StkP/MapZ and DivIVA during Mn toxicity (Fig. 4A–B), with the highly Mn-sensitive double mutant *psaR mntE* characterized by 45% less phosphorylated DivIVA than WT. Diminished Thr-phosphorylation does not result from lower protein expression, since StkP, MapZ, and DivIVA all show robust WT-like protein concentrations independent of Mn stress

(Fig. S6B–D). These results suggest that PhpP phosphatase activity is increased during Mn toxicity and that a *phpP*-null mutation might rescue DivIVA phosphorylation levels. Unfortunately, a *phpP*-null strain could not be obtained without the acquisition of suppressor mutations in StkP that reduce StkP expression or activity (Rued *et al.*, 2016); this results in overall lower StkP/MapZ and DivIVA phosphorylation levels compared to the WT strain (Fig. 4C–D, *black* bars). Despite this, Mn stress has no effect on phosphorylation levels in the absence of *phpP* (Fig. 4C–D), consistent with the hypothesis that hyperactivation of PhpP during Mn stress is responsible for the observed decrease in phosphorylated StkP/MapZ and DivIVA.

We further examined the effect of the loss of DivIVA phosphorylation on growth during Mn stress using viable strains harboring either a *divIVA*-null mutation or a non-phosphorylatable *divIVA*-(T201A) allele. Both the single *divIVA*-null and the *divIVA*-(T201A) mutants mimic WT-like growth and are insensitive to Mn stress (Fig. S7). Cell morphology is similar to those reported previously by others (Fadda *et al.*, 2003; Fadda *et al.*, 2007; Boersma *et al.*, 2015), where *divIVA* mutants characteristically form long chains of aberrant cells and *divIVA*-(T201A) cells appear WT-like with no morphological changes. The double mutants, *mntE divIVA* and *mntE divIVA*-(T201A), also grew similar to WT in BHI. During Mn stress, *mntE divIVA* mutants showed a longer growth arrest before growth resumption than *mntE* alone, whereas *mntE divIVA*-(T201A) grew similar to that of *mntE* (Fig. S7B). These data are consistent with a lack of effect of DivIVA phosphorylation on cell division in pneumococcal D39 (Massidda *et al.*, 2013). Taken together, these data show that Mn availability strongly affects cell morphology as a result of perturbation of protein phosphorylation status by the StkP kinase/PhpP phosphatase pair.

Bioavailable Mn:Zn ratio regulates PhpP phosphatase activity

One possible explanation for what appears to be hyperactive PhpP phosphatase activity in cells is over-metallation with Mn, relative to other divalent metal ions that do not support robust catalytic activity. To test this, we measured the specific activities of various metalloderivatives of purified pneumococcal PhpP. Based on structural work on other bacterial type 2C protein phosphatase (PP2C) superfamily members (Pullen *et al.*, 2004; Rantanen *et al.*, 2006; Wehenkel *et al.*, 2007; Schlicker *et al.*, 2008; Su *et al.*, 2011), *S. pneumoniae* PhpP is predicted to bind three metal ions coordinated by conserved aspartate residues, with two metal ions (M1 and M2) forming a binuclear active site harboring the bridging water nucleophile (Fig. S8A). Binding of the third metal ion (M3) remains controversial, since its coordination is variable among PP2C superfamily members and solution studies often fail to confirm its presence (Pullen *et al.*, 2004; Rantanen *et al.*, 2007; Wehenkel *et al.*, 2007; Schlicker *et al.*, 2008; Su *et al.*, 2011). Moreover, Ala substitution of the same M3 coordinating Asp residue reveals no significant impact in phosphatase activity in the *Mycobacterium tuberculosis* PP2C PstP (Wehenkel *et al.*, 2007) but a significant impairment of the *Thermosynechococcus elongatus* PphA catalytic activity (Su *et al.*, 2011). In any case, bacterial PP2C phosphatases do bind metal cations and are preferentially activated by Mn (Mukhopadhyay *et al.*, 1999; Obuchowski *et al.*, 2000; Treuner-Lange *et al.*, 2001; Novakova *et al.*, 2005). Here, we show *in vitro* that purified apo-PhpP binds two metal mol•equiv of Zn vs. one mol•equiv of Mn in competition with a modest affinity competitor

chelator, mag-fura-2 (mf2) (Fig. S8B–C). A second Mn that does not compete with mf2 can only be detected in kinetic assays (see below), and is characterized by log $K_{a2} \leq 4.0$, an upper limit from the mf2 titrations (Fig. S8B–C). While the association equilibrium constants (K_{Me}) for the metal-binding site 1 differ by two orders of magnitude for Mn (log K_{a1} 5.24±0.07) vs. Zn (log K_{a1} 7.74±0.03), the site 2 affinity is at least three orders of magnitude larger for Zn (log K_{a2} 6.93±0.04) relative to Mn. These data reveal Zn binds more tightly to both sites 1 and 2 in PhpP than Mn, a finding consistent with predictions from the Irving-William series of metal complex stabilities (Irving and Williams, 1948). However, the larger disparity between the K_{Zn} and the K_{Mn} values for site 2 suggests that site 2 (or both sites 2 and 3; our data do not distinguish between these possibilities) is a likely regulatory site that dictates functional assembly of the binuclear cluster in PhpP and therefore enzyme activity in cells. Thus, a modest change in the bioavailable Mn:Zn ratio is likely capable of modulating the specific activity of PhpP *in vivo*.

We confirmed this *in vitro* by assessing how Mn:Zn and Mn:Fe ratios influence PhpP phosphatase activity using the phosphopeptide RRA(pT)VA as substrate. Titration of Mn(II) into apo-PhpP resulted in a Mn-dependent increase in PhpP phosphatase specific activity, with 2 mM Mn optimal under our conditions (Fig. 5A); thus, filling site 2 is clearly required for maximum PhpP activity. Mg(II) and Fe(II) were significantly less effective than Mn(II) in activating PhpP (Fig. 5B), and no activity was observed with Zn(II). Other transition metals, such as nickel and cobalt, were not tested here because only trace amounts of these metals are found associated with pneumococcal cells (Manzoor *et al.*, 2015b; Jacobsen *et al.*, 2011; Manzoor *et al.*, 2015a) and will therefore not outcompete Mn, Zn, or Fe *in vivo* under unstressed conditions. Addition of Zn(II) to Mn-PhpP results in a significant decrease in PhpP activity (Fig. 5C), while excess Fe(II) does not impact Mn-dependent PhpP phosphatase activity (Fig. 5D); both findings are consistent with previous work . Note that Mn-dependent PhpP phosphatase activity remains relatively unchanged when up to 2-fold excess Fe(II) to Mn(II) (similar to that of the cell-associated Mn:Fe ratio shown in Fig. 1E for Mn-stressed *mntE* cells) is provided, suggesting that the observed *in vivo* elevated Fe levels do not significantly impact PhpP activity. In contrast to Fe(II), these data suggest that PhpP specific activity can be precisely controlled by the bioavailable Mn:Zn ratio *in vivo*.

DISCUSSION

The work presented here provides novel insights as to why some pathogenic bacteria express a highly specific Mn efflux transporter (Rosch *et al.*, 2009; Martin and Giedroc, 2016) despite the fact that most, including *S. pneumoniae*, will only intermittently encounter significant Mn toxicity when switching between niches during the course of infection. We suggest that dysregulation of intracellular Mn homeostasis, independent of an oxidative stress response, significantly impacts cell division via alteration of the metallation status of the phosphatase PhpP, and therefore the steady-state phosphorylation status of key target proteins (Fig. 6). Hyperactivation of PhpP as a result of over-metallation by excess Mn leads to reduced phosphorylation status, resulting in elongated, asymmetrically dividing, and highly chained cells. In contrast, inhibition of PhpP as a result of Zn toxicity increases net phosphorylation, thus leading to a shortened cell morphology. These findings are consistent with our proposal that Mn metalloenzymes in cells are metallated by default, such that the

pool of bioavailable metals can properly “tune” the specific activity in a window that is compatible with cellular regulation (Tottey *et al.*, 2008).

The specific features of this metallostasis model as they relate to dysregulation of a bacterial phosphatase-kinase signaling pair likely has precedence in other PP2C superfamily phosphatases. For example, Mn levels are known to influence the activation of the sigma B general stress response in both *B. subtilis* and *Staphylococcus aureus* by stimulating the PP2C phosphatase RsbU (Guedon *et al.*, 2003; Pane-Farre *et al.*, 2006). In contrast, elevated Zn levels affect spore germination by inhibiting activity of the PrpP phosphatase in *B. anthracis*; PrpP inhibition therefore promotes PrkP kinase activity and further downstream substrate phosphorylation (Arora *et al.*, 2013).

It will be interesting to determine if this metallostasis model (Fig. 6) characterizes another pneumococcal Mn phosphatase-kinase pair, CpsB/CpsD, involved in the regulation of the biosynthesis of the polysaccharide capsule, or PpaC, the Mn-dependent inorganic pyrophosphatase, both of which are required for full virulence of *S. pneumoniae*. In the latter case, cellular Mn status would influence inorganic phosphate speciation, potentially controlling the formation of low molecular weight Mn-phosphate complexes, which are known superoxide dismutase and catalase mimetics (Culotta and Daly, 2013). This, in fact, potentially explains the reduced H_2O_2 loads in Mn-stressed pneumococcal cells (Fig. S3).

Our data also reveal the striking finding that the Mn and Fe quotas of *S. pneumoniae* are dramatically altered in an oxygen-dependent manner. The cell-associated Mn concentration is 10-fold lower (≈100 to 10 ng/mg protein) while Fe increases significantly (≈100 to 600 ng/mg protein) in anaerobically grown wild-type cells, suggesting that *S. pneumoniae* switches from a Mn-centric (Mn:Fe ratio =1) to an Fe-centric (Mn:Fe ratio ≤1) metabolism in the absence of oxygen (Lisher and Giedroc, 2013). Furthermore, Mn toxicity leads to diminished Fe levels under anaerobic conditions (Fig. 2C), similar to that observed aerobically for the Fe-centric bacterium *E. coli* (Martin *et al.*, 2015). During infection and disease progression from pneumonia to bacteremia to meningitis, oxygen availability diminishes, while total Fe levels increase at mammalian host sites of infection (McDevitt *et al.*, 2011). The extent to which this Fe or other transition metals is bioavailable is unknown; however, small fluctuations in bioavailable metal could induce mismetallation of both transcriptional regulatory proteins and metalloenzymes (Lisher *et al.*, 2017), which can drive either inactivation or inappropriate hyperactivation as demonstrated here with PhpP.

It is also possible that excess Mn might inhibit Fe entry into the sulfur formation system (Suf) thereby inhibiting iron-sulfur cluster biogenesis and depleting Fe stores further. Although poorly explored, *S. pneumoniae* does encode a limited number of known Fe-S requiring radical-SAM (*S*-adenosylmethionine) enzymes several of which are necessary for anaerobic growth, with transcription of the Suf system induced with a switch from anaerobic to aerobic growth (Lisher *et al.*, 2017). In *E. coli*, Fe and Mn compete for the metal-binding site of the Mn-dependent superoxide dismutase SodA. Incorrect incorporation of Fe into SodA produces an enzyme with peroxidase-catalase activity that was observed to increase cell susceptibility to hydrogen peroxide via protein oxidation (Ganini *et al.*, 2015). As a lactic acid bacterium, *S. pneumoniae* produces significant endogenous hydrogen peroxide,

up to ≈0.4 mM (Fig. S3), resulting in significant proteome thiol sulfenylation (Lisher *et al.*, 2017). In contrast to *E. coli*, we observe that SOD activity is unaffected by Mn toxicity. High copper concentrations during aerobic growth could possibly inactivate SodA as there is speculation to suggest that Mn-dependent enzymes can also bind Cu, rendering them inactive (Johnson *et al.*, 2015). Additional studies are clearly required to ascertain the specifics of a Mn-Cu interconnection in cells.

The interdependence of bioavailable Zn and Mn, in contrast, is much better understood. In this study, we find that the relative bioavailability of Mn versus Zn is a key determinate in global regulatory processes, *i.e.,* regulation of protein activity by reversible phosphorylation. Too much Mn leads to hyperactivation of PhpP phosphatase activity, whereas Zn inhibits this activity. These findings highlight a direct connection between metal homeostasis and the regulation of cell division, and perhaps more broadly, the regulation of cellular specific activities of other Mn metalloenzymes (Fig. 6). In other bacteria, global metal-dependent transcriptional regulators, including Fur and PerR, do not impact the activity of other enzymes directly, but rather regulate expression of genes that allow an organism to adapt to changes in metal bioavailability and reactive oxygen species (ROS). There are no known Fur-like homologues present in *S. pneumoniae*, and we have suggested that part of this adaptive response to endogenous ROS is chemical adaptation via protein sulfenylation (Lisher *et al.*, 2017). Alternatively or in addition, *S. pneumoniae* may employ two-component kinase-response regulator signal transduction pairs (TCSs) to effect Fe-regulation, perhaps through RitR, an orphan response regulator (Ulijasz *et al.*, 2009). The structure of the RitR regulatory domain demonstrates that RitR lacks the key Asp residue involved in the phosphoryl signal relay process in other TCSs (Maule *et al.*, 2015) and it is unknown whether RitR activation is influenced by changes in intracellular transition metal.

A number of recent reports have used the Zn-inducible *sczA-czcD* intergenic operator-promoter region (P_{Zn}) to control expression of heterologous genes of interest (Fleurie *et al.*, 2014b; Fenton *et al.*, 2016; Ulrych *et al.*, 2016). The studies reported here suggest caution when using this approach, particularly since Zn is a highly competitive metal that has the potential to displace more weakly bound first-row transition metals, like Mn, from protein active sites (Braymer and Giedroc, 2014; Ong *et al.*, 2015). Supplementation of a rich medium with as little as 0.2 mM extracellular Zn gives rise to a detectable morphological change (Fig. 3) and a clear growth phenotype for the encapsulated *S. pneumoniae* D39 strain (Reyes-Caballero *et al.*, 2010; Martin and Giedroc, 2016). Moreover, Zn-toxicity within infected macrophages is clearly implicated as a host-mediated strategy by which the innate immune response exploits the chemistry of zinc to aid in the clearance of invasive bacterial pathogens (Martin *et al.*, manuscript in preparation). Supplementation with Mn may relieve the growth phenotype observed during Zn toxicity but the extent to which metabolic processes remain affected by high levels of extracellular Zn or Mn is unclear.

In summary, our findings provide the first clues to the molecular targets of manganese toxicity in a bacterial pathogen. The data presented here significantly extend our understanding of why bacterial cells express a Mn-specific efflux pump and are consistent with a hyperactivation model of Mn toxicity. Much of the ongoing work in transition metal homeostasis has to date focused on host-derived deprivation of key micronutrients, termed

nutritional immunity, and how pathogenic bacteria adapt and overcome severe host-mediated metal starvation. For Mn and Zn, the primary mechanism centers on a set of S100 proteins that have the ability to chelate various divalent ions in a calcium-activated fashion and withhold them from the invading pathogen, of which calprotectin is the best studied (Zackular *et al.*, 2015). We suggest that adaptation to stress induced by dysregulation of both arms of Mn homeostasis, limitation and toxicity, impacts the physiology and virulence of bacterial pathogens and thus may represent an fertile area for the development of new therapeutics that target manganese homeostasis systems.

EXPERIMENTAL PROCEDURES

Reagents

All antibiotics, bicinchoninic acid, desferrioxamine, ferrous ammonium sulfate, manganese (II) chloride tetrahydrate, nitrilotriacetic acid (NTA), reduced or oxidized glutathione, and xanthine was purchased from Sigma-Aldrich; zinc sulfate and cytochrome *c* from equine heart from Alfa Aesar; TraceSELECT® nitric acid (HNO_3), from Fluka; xanthine oxidase from Calbiochem; filtered catalase from Worthington biochemical; Bacto™ brain heart infusion broth (BHI) and BBL™ trypticase™ soy agar with sheep blood were purchased from Becton Dickinson; and the Ser/Thr phosphatase assay system containing the phosphopeptide, RRA(pT)VA from Promega.

Bacterial strain and plasmid construction

The strains used in this study were derived from *S. pneumoniae* D39 (IU1781) and are listed in Table S1. All *S. pneumoniae* mutants were constructed by gene deletion replacement and counter antibiotic selection using the *rpsL*$^+$ cassette, Janus (Sung *et al.*, 2001). Briefly, the 0.8 to 1-kb region upstream and downstream of target genes were amplified from genomic DNA using inner primers containing flanking regions to the kanamycin-resistant Janus cassette (*kan-rpsL*$^+$). The two outside fragments generated were then joined together with the inner *kan-rpsL*$^+$ fragment. The final PCR product was transformed into competent *rpsL1* pneumococcal cells using standard techniques (Tsui *et al.*, 2010). Bacteria were grown on trypticase soy agar II plates containing 5% (v/v) defibrinated sheep blood (TSAII-BA). Plates were incubated at 37°C in an atmosphere of 5% CO_2. For antibiotic selections, TSAII-BA plates contained 250 μg/ml kanamycin or streptomycin.

Plasmid pPhpP8 was constructed by amplifying *phpP* (SPD_1543) from *S. pneumoniae* D39 genomic DNA using the forward 5′-GGACTGACGCCA TGGAAATCTCAT-′3 and reverse 5′-GTAGTTGGTCCTCTGAATTCTCACTCACAC-′3 primers (restriction sites are underlined). The PCR product was digested with NcoI and EcoRI, cloned into pHis-Parallel behind a T7 promoter, and transformed into *E. coli* DH5α. The resulting construct was sequence verified and transformed into *E. coli* Rosetta pLysS for expression and purification of PhpP.

Growth conditions for *S. pneumoniae*

Brain-heart infusion (BHI) medium was of standard composition and prepared with double distilled water. Standard BHI broth contained 200 nM Mn in final preparation. For growth

experiments, bacteria were inoculated into BHI broth from frozen culture stocks, then serially diluted and propagated overnight at 37°C. Overnight exponentially growing cultures were diluted to 0.005 OD_{620} into pre-warmed BHI containing increasing concentrations of $MnCl_2$. All aerobic cell growth experiments were monitored over time at 37°C in an atmosphere of 5% CO_2. Anaerobic cell growth was monitored over time in an anaerobic chamber (Coy Laboratory Products Inc.) in an atmosphere of 85% N_2, 10% H_2, and 5% CO_2.

Inductively coupled plasma-mass spectrometry (ICP-MS) for measurement of total cell-associated metal

The total amounts of cell-associated Mn, Fe, Zn or Cu were quantified from 5–20 mL cultures that had been grown in BHI with or without 0.2 mM $MnCl_2$ for 3.5 h. Cells were centrifuged, washed once with ice-cold phosphate buffered saline (PBS), pH 7.4 containing 2 mM NTA, washed twice with ice-cold metal-free PBS (10g/L chelex-100 resin was used to remove metals), pH7.4, and dried overnight using a centrifuge evaporator. Dried cells were solubilized in 400 μL 30% (v/v) HNO_3 and lysed by incubating at 95°C for 10 min shaking at 500 rpm. ICP-MS samples were prepared by diluting 300 μL of lysed cells into 2.7 ml 2.5% (v/v) HNO_3. Metal concentrations were calculated from the standard curve using 1 to 30 ppb metal stock solutions and normalized to total protein determined using DC™ protein assay (Biorad).

Hydrogen peroxide production

Overnight cultures were diluted into 5 mL pre-warmed BHI broth with or without 0.1 mM $MnCl_2$ and incubated at 37°C in an atmosphere of 5% CO_2. Cells were harvested at approximately 0.3 OD_{620} by centrifugation, washed once with ice-cold PBS, pH 7.4, and suspended in 5 mL PBS, pH 7.4 containing 0.5 mM glucose. Cells were incubated at 37°C or 32°C in an atmosphere of 5% CO_2 for 1 h, then centrifuged, and the supernatant was filtered through a 0.2 μm syringe filter. The concentration of H_2O_2 produced by cells was determined from the filtered supernatant using the Pierce™ Quantitative Peroxide Assay kit (Life Technologies) according to the directions supplied. Briefly, samples were diluted 1/50 into 200 μL working reagent (100 mM sorbitol, 25 mM H_2SO_4, 250 μM ammonium ferrous sulfate, 125 μM xylenol orange) and incubated for 20 min at room temperature. Product produced was measured spectrophotometrically at 595 nm and the total amount of H_2O_2 produced was quantified using a standard curve prepared with known concentrations of H_2O_2.

RNA isolation

Total RNA was isolated from cells by hot phenol extraction (Martin and Imlay, 2011). Briefly, an aliquot of cells was mixed with pre-warmed fresh 8× lysis solution (0.32 M Na-acetate pH 5.5, 0.4% SDS, 16 mM EDTA, pH 8 in DEPC water) containing saturated phenol and incubated at 65°C for 15 min, shaking at 1400 rpm. After microcentrifugation at room temperature for 10 min, the aqueous layer was transferred to a clean tube, and several phenol-chloroform extractions were performed. Extracted RNA was ethanol precipitated from the aqueous layer and incubated at −80°C overnight. Samples were microcentrifuged at max speed for 10 min at 4°C. Precipitated RNA was rinsed with cold 75% ethanol by gentle

palpitation, air dried, suspended in 10 mM Tris, 1 mM EDTA (RNase free) buffer, pH 7, and stored at −80°C. Contaminating DNA was removed from isolated RNA by rigorous DNase treatment using the Turbo DNA-*free*™ kit (Ambion) according to the manufacturer's guidelines. The RNA product was confirmed DNA-free using PCR and gel electrophoresis. DNA-free RNA (125 ng) was converted to cDNA by reverse transcription using qScript™ cDNA synthesis kit (Quanta Biosciences) according to the manufacturer's guidelines.

Quantitative real-time PCR

PCR amplification was carried out using the primer pairs listed in Table S2. *gyrA* served as the housekeeping gene (Kazmierczak *et al.*, 2009). PCR amplification was performed in a mixture (20 µl final volume) containing 2× SYBR Green QPCR master mix (Agilent technologies), 250 nM each primer and 1/30 dilution cDNA. Cycling conditions were as follows: 95°C/3 min; 40 cycles of 95°C/20 s, 59°C/20 s. PCR outcomes were normalized to the *gyrA* gene and relative transcription levels were calculated by comparison of the ratio of treated to non-treated cells.

Cell morphology measurements

The lengths and widths of cells growing in BHI broth with or without $MnCl_2$ or $ZnSO_4$ were measured from phase-contrast images using Nikon NIS-Element AR software ENREF 36 (Barendt *et al.*, 2009). Approximately 100 to 300 or more cells were measured for each strain. *P*-values were obtained by student *t*-test (unpaired test with Welch's correction) or one-way ANOVA analysis (nonparametric Kruskal-Wallis test) using GraphPad Prism.

Measuring threonine-phosphorylated proteins by western blot

Protein phosphorylation was performed by modification of a previously published protocol (Novakova *et al.*, 2010). Briefly, overnight cultures were diluted into 5 mL pre-warmed BHI broth with or without 0.1 mM $MnCl_2$ and incubated at 37°C in an atmosphere of 5% CO_2. Cells were harvested at approximately 0.2 OD_{620} by centrifugation, washed once with ice-cold PBS, pH 7.4, and suspended in 200 µL 1x SEDS buffers (0.1% deoxycholate, 150 mM NaCl, 0.2% SDS, 15 mM EDTA in ddH_2O). Cell suspension was vigorously vortexed and lysis was allowed to occur for 30 min at 37°C. Microscopy was used to confirm complete cell lysis. Protein content was determined using the D™ Protein Assay and equal amount of protein (10 µg) were analyzed by western blot. Phosphorylated threonine amino acids were probed by phospho-threonine rabbit polyclonal antibodies (Cell Signaling Technology). Proteins were detected using an anti-rabbit donkey-horseradish peroxidase conjugated antibody and ECL western blotting detection reagents (GE Healthcare). Western blots were imaged using an image vision system.

Western blot analysis of protein expression

Protein expression was determined from strains harboring chromosomal fusions of C-terminal FLAG-tagged StkP, MapZ, and DivIVA proteins grown in BHI with or without 200 µM $MnCl_2$ for 3.5 h. Cells were centrifuged, washed with ice-cold PBS, pH 7.4, resuspended in 1/35 the original culture volume with PBS, pH 7.4 containing 1% sodium dodecyl sulfate, 0.1% triton X-100 and 0.5 mg DNase, and lysed at 37°C for 10 min. Cell

lysates were diluted into 2x Laemmli sample buffer (Biorad) containing β-mercaptoethanol and heated at 95°C for 10 min. 10–15 μg total proteins were separated by SDS-PAGE and transferred to a nitrocellulose membrane. Membranes were blocked with 5% membrane block agent (ECL, GE Healthcare) in PBS, pH 7.4 containing 0.1% Tween 20 (PBST) and probed with anti-FLAG rabbit polyclonal antibody in PBST. Proteins were detected using anti-rabbit antibody linked to horse radish peroxidase and ECL western blotting reagent. Western blots were imaged using an image vision system.

Expression and purification of *S. pneumoniae* PhpP

Overnight *E. coli* Rosetta pLysS cells harboring pPhpP8 were diluted 1/100 into fresh LB medium containing 100 μg/mL ampicillin and grown aerobically at 30°C. At approximately 0.6 OD_{600}, 1 mM isopropyl β-D-1-thiogalactopyranoside was added to induce *S. pneumoniae* PhpP protein synthesis. One-liter of cells were harvested after 3 h by centrifugation. Cells were suspended in low imidazole buffer (25 mM Tris-HCl, pH 7.5, 500 mM NaCl, 3 mM tris(2-carboxyethyl) phosphine (TCEP), 20 mM imidazole) and disrupted by sonication on ice (1/2 in. probe at 30 % power for 36 cycles, 15 s pulse). Cell debris was removed by centrifugation and purified by gravity flow over a Ni(II)-NTA affinity column pre-equilibrated with low imidazole buffer. Bound proteins were eluted with high imidazole buffer (25 mM Tris-HCl, pH 7.5, 500 mM NaCl, 3 mM TCEP, 500 mM imidazole). The His_6-N-terminal tag was removed from pooled fractions of protein by incubation with lab purified Tobacco Etch Virus (TEV) protease at 4°C for 48 h. The buffer was exchanged back to low imidazole (20 mM) and flowed thru Ni(II)-NTA affinity column by gravity flow. Fractions containing His_6-tag free proteins were pooled, concentrated, and separated further on a HiLoad 16/600 Superdex 75 size-exclusion column (GE Healthcare) equilibrated with 25 mM Hepes, pH8.0, 200 mM NaCl, 3 mM TCEP, 5 mM EDTA buffer. Fractions containing PhpP were pooled and concentrated. EDTA was removed using a gravity flow desalting column and divalent metal cations were removed by dialyzing protein against 25 mM Hepes, pH 8.0, 100 mM NaCl, 3 mM TCEP buffer containing 10 g/L Chelex-100 resin. Purity of protein was visualized by 15 % polyacrylamide gel electrophoresis. Mass spectrophotometry (ESI-MS and MALDI-TOF) was performed to confirm the identity of the final protein isolated using established laboratory procedures. Protein concentrations were calculated using a predicted extinction coefficient 21430 M^{-1} cm^{-1} at 280 nm (Protparam) (Gasteiger *et al.*, 2005). Final protein yield was approximately 1 g/L of cell culture.

Metal-binding stoichiometry and affinity determinations

Purified apo-PhpP was diluted into metal-free buffer (25 mM Hepes, pH 8.0, 100 mM NaCl). A fixed concentration of metal-free mag-fura-2 (MF2) was added to the solution to reach a final volume of 1 mL. Metal stocks of Mn(II) and Zn(II) were titrated into the protein-competitor solution and the absorbance at 360 nm and 325 nm were monitored which report on the λmax for the metal-free and metal-bound states of the MF2 (Lisher *et al.*, 2013), respectively, were taken after 2 min incubation. All metal binding experiments were acquired with a Hewlett-Packard model 8452A spectrophotometer at room temperature. The MF2 binding curves were fitted to an appropriate one-step competition binding model using Dynafit (Kuzmic, 1996).

Phosphatase assay

The phosphatase activity of purified PhpP toward the chemically synthesized phosphopeptide, RRA(pT)VA, substrate was measured using the serine/threonine phosphatase assay system (Promega). The standard assay was carried out in a final volume of 50 μL metal-free buffer (25 mM Hepes, pH 8.0 containing 100 mM NaCl), 100 μM phosphopeptide substrate, metal cation, and 730 nM of apo-PhpP at 37°C for 30 min. The reaction was terminated by the addition of 50 μL molybdate dye/additive mixture and allowed to develop at room temperature for 15 min. Released inorganic phosphate (P_i) was detected spectrophotometrically at 600 nm. The amount of P_i released was determined using a standard curve prepared with known concentrations of P_i. All Fe(II) titrations were carried out in an anaerobic chamber (Coy Laboratory Products Inc.) in an atmosphere of 85% N_2, 10% H_2, and 5% CO_2.

Supplementary Material

Refer to Web version on PubMed Central for supplementary material.

Acknowledgments

We greatly thank Britta Rued and H. Tiffany Tsui for providing strain information and help with the threonine-phosphorylation detection method. This work was supported by NIH grants GM042569 and GM118157 (to D.P.G.), GM113172 and GM114315 (to M.E.W.), and supplemental grant award GM042569-25S1 (to J.E.M.).

References

Arora G, Sajid A, Arulanandh MD, Misra R, Singhal A, Kumar S, Singh LK, Mattoo AR, Raj R, Maiti S, Basu-Modak S, Singh Y. Zinc regulates the activity of kinase-phosphatase pair (BasPrkC/BasPrpC) in *Bacillus anthracis*. Biometals. 2013; 26:715–730. [PubMed: 23793375]

Barendt SM, Land AD, Sham LT, Ng WL, Tsui HC, Arnold RJ, Winkler ME. Influences of capsule on cell shape and chain formation of wild-type and *pcsB* mutants of serotype 2 *Streptococcus pneumoniae*. J Bacteriol. 2009; 191:3024–3040. [PubMed: 19270090]

Beilharz K, Novakova L, Fadda D, Branny P, Massidda O, Veening JW. Control of cell division in S*treptococcus pneumoniae* by the conserved Ser/Thr protein kinase StkP. Proc Natl Acad Sci U S A. 2012; 109:E905–913. [PubMed: 22431591]

Boersma MJ, Kuru E, Rittichier JT, VanNieuwenhze MS, Brun YV, Winkler ME. Minimal peptidoglycan (PG) turnover in wild-type and PG hydrolase and cell division mutants of *Streptococcus pneumoniae* D39 growing planktonically and in host-relevant biofilms. J Bacteriol. 2015; 197:3472–3485. [PubMed: 26303829]

Braymer JJ, Giedroc DP. Recent developments in copper and zinc homeostasis in bacterial pathogens. Curr Opin Chem Biol. 2014; 19:59–66. [PubMed: 24463765]

Counago RM, Ween MP, Begg SL, Bajaj M, Zuegg J, O'Mara ML, Cooper MA, McEwan AG, Paton JC, Kobe B, McDevitt CA. Imperfect coordination chemistry facilitates metal ion release in the Psa permease. Nat Chem Biol. 2014; 10:35–41. [PubMed: 24212134]

Culotta VC, Daly MJ. Manganese complexes: diverse metabolic routes to oxidative stress resistance in prokaryotes and yeast. Antioxid Redox Signal. 2013; 19:933–944. [PubMed: 23249283]

Dintilhac A, Alloing G, Granadel C, Claverys JP. Competence and virulence of *Streptococcus pneumoniae*: Adc and PsaA mutants exhibit a requirement for Zn and Mn resulting from inactivation of putative ABC metal permeases. Mol Microbiol. 1997; 25:727–739. [PubMed: 9379902]

Dworkin J. Ser/Thr phosphorylation as a regulatory mechanism in bacteria. Curr Opin Microbiol. 2015; 24:47–52. [PubMed: 25625314]

Echlin H, Frank MW, Iverson A, Chang TC, Johnson MD, Rock CO, Rosch JW. Pyruvate Oxidase as a Critical Link between Metabolism and Capsule Biosynthesis in Streptococcus pneumoniae. PLoS Pathog. 2016; 12:e1005951. [PubMed: 27760231]

Eijkelkamp BA, Morey JR, Ween MP, Ong CL, McEwan AG, Paton JC, McDevitt CA. Extracellular zinc competitively inhibits manganese uptake and compromises oxidative stress management in *Streptococcus pneumoniae*. PloS One. 2014; 9:e89427. [PubMed: 24558498]

Fadda D, Pischedda C, Caldara F, Whalen MB, Anderluzzi D, Domenici E, Massidda O. Characterization of *divIVA* and other genes located in the chromosomal region downstream of the *dcw* cluster in *Streptococcus pneumoniae*. J Bacteriol. 2003; 185:6209–6214. [PubMed: 14526035]

Fadda D, Santona A, D'Ulisse V, Ghelardini P, Ennas MG, Whalen MB, Massidda O. *Streptococcus pneumoniae* DivIVA: localization and interactions in a MinCD-free context. J Bacteriol. 2007; 189:1288–1298. [PubMed: 17098892]

Fenton AK, Mortaji LE, Lau DT, Rudner DZ, Bernhardt TG. CozE is a member of the MreCD complex that directs cell elongation in Streptococcus pneumoniae. Nat Microbiol. 2016; 2:16237. [PubMed: 27941863]

Fisher S, Buxbaum L, Toth K, Eisenstadt E, Silver S. Regulation of manganese accumulation and exchange in Bacillus subtilis W23. J Bacteriol. 1973; 113:1373–1380. [PubMed: 4347971]

Fleurie A, Lesterlin C, Manuse S, Zhao C, Cluzel C, Lavergne JP, Franz-Wachtel M, Macek B, Combet C, Kuru E, VanNieuwenhze MS, Brun YV, Sherratt D, Grangeasse C. MapZ marks the division sites and positions FtsZ rings in *Streptococcus pneumoniae*. Nature. 2014a; 516:259–262. [PubMed: 25470041]

Fleurie A, Manuse S, Zhao C, Campo N, Cluzel C, Lavergne JP, Freton C, Combet C, Guiral S, Soufi B, Macek B, Kuru E, VanNieuwenhze MS, Brun YV, Di Guilmi AM, Claverys JP, Galinier A, Grangeasse C. Interplay of the serine/threonine-kinase StkP and the paralogs DivIVA and GpsB in pneumococcal cell elongation and division. PLoS Genet. 2014b; 10:e1004275. [PubMed: 24722178]

Fu Y, Tsui HCTH, Bruce KE, Sham LTL, Higgins KA, Lisher JP, Kazmierczak KM, Maroney MJ, Dann CE, Winkler ME, Giedroc DP. A new structural paradigm in copper resistance in *Streptococcus pneumoniae*. Nat Chem Biol. 2013; 9:177–183. [PubMed: 23354287]

Fuangthong M, Herbig AF, Bsat N, Helmann JD. Regulation of the *Bacillus subtilis fur* and *perR* genes by PerR: not all members of the PerR regulon are peroxide inducible. J Bacteriol. 2002; 184:3276–3286. [PubMed: 12029044]

Ganini D, Petrovich RM, Edwards LL, Mason RP. Iron incorporation into MnSOD A (bacterial Mn-dependent superoxide dismutase) leads to the formation of a peroxidase/catalase implicated in oxidative damage to bacteria. Biochim Biophys Acta. 2015; 1850:1795–1805. [PubMed: 25964067]

Gasteiger, E., Hoogland, C., Gattiker, A., Duvaud, S., Wilkins, MR., Appel, RD., Bairoch, A. Protein identification and analysis tools on the ExPASy server. In: Walker, JM., editor. The proteomics protocols handbook. Humana Press; 2005. p. 571-607.

German N, Luthje F, Hao X, Ronn R, Rensing C. Microbial Virulence and Interactions With Metals. Prog Mol Biol Transl Sci. 2016; 142:27–49. [PubMed: 27571691]

Guedon E, Moore CM, Que Q, Wang T, Ye RW, Helmann JD. The global transcriptional response of Bacillus subtilis to manganese involves the MntR, Fur, TnrA and sigmaB regulons. Mol Microbiol. 2003; 49:1477–1491. [PubMed: 12950915]

Helmann JD. Specificity of metal sensing: iron and manganese homeostasis in *Bacillus subtilis*. J Biol Chem. 2014; 289:28112–28120. [PubMed: 25160631]

Higgins, KA., Giedroc, DP. Encyclopedia of Inorganic and Bioinorganic Chemistry. Chichester, UK: John Wiley & Sons, Ltd; 2013. Metal Specificity of Metallosensors; p. 1-16.

Honsa ES, Johnson MD, Rosch JW. The roles of transition metals in the physiology and pathogenesis of *Streptococcus pneumoniae*. Front Cell Infect Biol. 2013; 3:92.

Huang X, Shin JH, Pinochet-Barros A, Su TT, Helmann JD. *Bacillus subtilis* MntR coordinates the transcriptional regulation of manganese uptake and efflux systems. Mol Microbiol. 2017; 103:253–268. [PubMed: 27748968]

Imlay JA. The mismetallation of enzymes during oxidative stress. J Biol Chem. 2014; 289:28121–28128. [PubMed: 25160623]

Irving H, Williams RJP. Order of stability of metal complexes. Nature. 1948; 162:746–747.

Jacobsen FE, Kazmierczak KM, Lisher JP, Winkler ME, Giedroc DP. Interplay between manganese and zinc homeostasis in the human pathogen *Streptococcus pneumoniae*. Metallomics. 2011; 3:38–41. [PubMed: 21275153]

Johnson MD, Kehl-Fie TE, Rosch JW. Copper intoxication inhibits aerobic nucleotide synthesis in *Streptococcus pneumoniae*. Metallomics. 2015; 7:786–794. [PubMed: 25730343]

Kazmierczak KM, Wayne KJ, Rechtsteiner A, Winkler ME. Roles of *rel*(Spn) in stringent response, global regulation and virulence of serotype 2 *Streptococcus pneumoniae* D39. Mol Microbiol. 2009; 72:590–611. [PubMed: 19426208]

Kelliher JL, Kehl-Fie TE. Competition for Manganese at the Host-Pathogen Interface. Prog Mol Biol Transl Sci. 2016; 142:1–25. [PubMed: 27571690]

Kuzmic P. Program DYNAFIT for the analysis of enzyme kinetic data: application to HIV proteinase. Anal Biochem. 1996; 237:260–273. [PubMed: 8660575]

Li N, Yang XY, Guo Z, Zhang J, Cao K, Han J, Zhang G, Liu L, Sun X, He QY. Varied metal-binding properties of lipoprotein PsaA in *Streptococcus pneumoniae*. J Biol Inorg Chem. 2014; 19:829–838. [PubMed: 24553956]

Lisher JP, Giedroc DP. Manganese acquisition and homeostasis at the host-pathogen interface. Front Cell Infect Biol. 2013; 3:91.

Lisher JP, Higgins KA, Maroney MJ, Giedroc DP. Physical characterization of the manganese-sensing pneumococcal surface antigen repressor from *Streptococcus pneumoniae*. Biochemistry. 2013; 52:7689–7701. [PubMed: 24067066]

Lisher JP, Tsui HC, Ramos-Montanez S, Hentchel KL, Martin JE, Trinidad JC, Winkler ME, Giedroc DP. Biological and chemical adaptation to endogenous hydrogen peroxide production in Streptococcus pneumoniae D39. mSphere. 2017; 2:e00291–00216. [PubMed: 28070562]

Manzoor I, Shafeeq S, Kloosterman TG, Kuipers OP. Co(2+)-dependent gene expression in *Streptococcus pneumoniae*: opposite effect of Mn(2+) and Co(2+) on the expression of the virulence genes *psaBCA*, *pcpA*, and *prtA*. Front Microbiol. 2015a; 6:748. [PubMed: 26257722]

Manzoor I, Shafeeq S, Kuipers OP. Ni2+-Dependent and PsaR-Mediated Regulation of the Virulence Genes *pcpA*, *psaBCA*, and *prtA* in *Streptococcus pneumoniae*. PloS One. 2015b; 10:e0142839. [PubMed: 26562538]

Marra A, Lawson S, Asundi JS, Brigham D, Hromockyj AE. In vivo characterization of the psa genes from *Streptococcus pneumoniae* in multiple models of infection. Microbiology. 2002; 148:1483–1491. [PubMed: 11988523]

Martin JE, Giedroc DP. Functional determinants of metal ion transport and selectivity in paralogous cation diffusion facilitator transporters CzcD and MntE in *Streptococcus pneumoniae*. J Bacteriol. 2016; 198:1066–1076. [PubMed: 26787764]

Martin JE, Imlay JA. The alternative aerobic ribonucleotide reductase of *Escherichia coli*, NrdEF, is a manganese-dependent enzyme that enables cell replication during periods of iron starvation. Mol Microbiol. 2011; 80:319–334. [PubMed: 21338418]

Martin JE, Waters LS, Storz G, Imlay JA. The *Escherichia coli* small protein MntS and exporter MntP optimize the intracellular concentration of manganese. PLoS Genet. 2015; 11:e1004977. [PubMed: 25774656]

Massidda O, Novakova L, Vollmer W. From models to pathogens: how much have we learned about *Streptococcus pneumoniae* cell division? Environ Microbiol. 2013; 15:3133–3157. [PubMed: 23848140]

Maule AF, Wright DP, Weiner JJ, Han L, Peterson FC, Volkman BF, Silvaggi NR, Ulijasz AT. The aspartate-less receiver (ALR) domains: distribution, structure and function. PLoS Pathog. 2015; 11:e1004795. [PubMed: 25875291]

McDevitt CA, Ogunniyi AD, Valkov E, Lawrence MC, Kobe B, McEwan AG, Paton JC. A molecular mechanism for bacterial susceptibility to zinc. PLoS Pathog. 2011; 7:e1002357. [PubMed: 22072971]

Morona JK, Morona R, Miller DC, Paton JC. *Streptococcus pneumoniae* capsule biosynthesis protein CpsB is a novel manganese-dependent phosphotyrosine-protein phosphatase. J Bacteriol. 2002; 184:577–583. [PubMed: 11751838]

Morrissey JA, Cockayne A, Brummell K, Williams P. The staphylococcal ferritins are differentially regulated in response to iron and manganese and via PerR and Fur. Infect Immun. 2004; 72:972–979. [PubMed: 14742543]

Mukhopadhyay S, Kapatral V, Xu W, Chakrabarty AM. Characterization of a Hank's type serine/threonine kinase and serine/threonine phosphoprotein phosphatase in *Pseudomonas aeruginosa*. J Bacteriol. 1999; 181:6615–6622. [PubMed: 10542161]

Novakova L, Bezouskova S, Pompach P, Spidlova P, Saskova L, Weiser J, Branny P. Identification of multiple substrates of the StkP Ser/Thr protein kinase in *Streptococcus pneumoniae*. J Bacteriol. 2010; 192:3629–3638. [PubMed: 20453092]

Novakova L, Saskova L, Pallova P, Janecek J, Novotna J, Ulrych A, Echenique J, Trombe MC, Branny P. Characterization of a eukaryotic type serine/threonine protein kinase and protein phosphatase of *Streptococcus pneumoniae* and identification of kinase substrates. FEBS J. 2005; 272:1243–1254. [PubMed: 15720398]

Obuchowski M, Madec E, Delattre D, Boel G, Iwanicki A, Foulger D, Seror SJ. Characterization of PrpC from *Bacillus subtilis*, a member of the PPM phosphatase family. J Bacteriol. 2000; 182:5634–5638. [PubMed: 10986276]

Ogunniyi AD, Mahdi LK, Jennings MP, McEwan AG, McDevitt CA, Van der Hoek MB, Bagley CJ, Hoffmann P, Gould KA, Paton JC. Central role of manganese in regulation of stress responses, physiology, and metabolism in *Streptococcus pneumoniae*. J Bacteriol. 2010; 192:4489–4497. [PubMed: 20601473]

Ong CL, Walker MJ, McEwan AG. Zinc disrupts central carbon metabolism and capsule biosynthesis in *Streptococcus pyogenes*. Sci Rep. 2015; 5:10799. [PubMed: 26028191]

Pane-Farre J, Jonas B, Forstner K, Engelmann S, Hecker M. The sigmaB regulon in *Staphylococcus aureus* and its regulation. Int J Med Microbiol. 2006; 296:237–258. [PubMed: 16644280]

Panosian TD, Nannemann DP, Watkins GR, Phelan VV, McDonald WH, Wadzinski BE, Bachmann BO, Iverson TM. *Bacillus cereus* phosphopentomutase is an alkaline phosphatase family member that exhibits an altered entry point into the catalytic cycle. J Biol Chem. 2011; 286:8043–8054. [PubMed: 21193409]

Papp-Wallace KM, Maguire ME. Manganese transport and the role of manganese in virulence. Ann Rev Microbiol. 2006; 60:187–209. [PubMed: 16704341]

Pericone CD, Park S, Imlay JA, Weiser JN. Factors contributing to hydrogen peroxide resistance in *Streptococcus pneumoniae* include pyruvate oxidase (SpxB) and avoidance of the toxic effects of the fenton reaction. J Bacteriol. 2003; 185:6815–6825. [PubMed: 14617646]

Pullen KE, Ng HL, Sung PY, Good MC, Smith SM, Alber T. An alternate conformation and a third metal in PstP/Ppp, the *M. tuberculosis* PP2C-Family Ser/Thr protein phosphatase. Structure. 2004; 12:1947–1954. [PubMed: 15530359]

Ramos-Montanez S, Tsui HC, Wayne KJ, Morris JL, Peters LE, Zhang F, Kazmierczak KM, Sham LT, Winkler ME. Polymorphism and regulation of the *spxB* (pyruvate oxidase) virulence factor gene by a CBS-HotDog domain protein (SpxR) in serotype 2 *Streptococcus pneumoniae*. Mol Microbiol. 2008; 67:729–746. [PubMed: 18179423]

Rantanen MK, Lehtio L, Rajagopal L, Rubens CE, Goldman A. Crystallization and preliminary crystallographic analysis of two *Streptococcus agalactiae* proteins: the family II inorganic pyrophosphatase and the serine/threonine phosphatase. Acta Crystallogr F. 2006; 62:891–894.

Rantanen MK, Lehtio L, Rajagopal L, Rubens CE, Goldman A. Structure of the *Streptococcus agalactiae* family II inorganic pyrophosphatase at 2.80 A resolution. Acta Crystallogr D. 2007; 63:738–743. [PubMed: 17505113]

Reyes-Caballero H, Guerra AJ, Jacobsen FE, Kazmierczak KM, Cowart D, Koppolu UM, Scott RA, Winkler ME, Giedroc DP. The metalloregulatory zinc site in *Streptococcus pneumoniae* AdcR, a zinc-activated MarR family repressor. J Mol Biol. 2010; 403:197–216. [PubMed: 20804771]

Rosch JW, Gao G, Ridout G, Wang YD, Tuomanen EI. Role of the manganese efflux system *mntE* for signalling and pathogenesis in *Streptococcus pneumoniae*. Mol Microbiol. 2009; 72:12–25. [PubMed: 19226324]

Rued BE, Zheng JJ, Mura A, Tsui HT, Boersma MJ, Mazny JL, Corona F, Perez AJ, Fadda D, Doubravová L, Branny P, Massidda O, Winkler ME. Suppression and synthetic-lethal genetic relationships of Δ*gpsB* mutations indicate that GpsB mediates protein phosphorylation and penicillin-binding protein interactions in *Streptococcus pneumoniae* D39. Mol Microbiol. 2016 in the press.

Schlicker C, Fokina O, Kloft N, Grune T, Becker S, Sheldrick GM, Forchhammer K. Structural analysis of the PP2C phosphatase tPphA from *Thermosynechococcus elongatus*: a flexible flap subdomain controls access to the catalytic site. J Mol Biol. 2008; 376:570–581. [PubMed: 18164312]

Su J, Schlicker C, Forchhammer K. A third metal is required for catalytic activity of the signal-transducing protein phosphatase M tPphA. J Biol Chem. 2011; 286:13481–13488. [PubMed: 21310952]

Sung CK, Li H, Claverys JP, Morrison DA. An *rpsL* cassette, Janus, for gene replacement through negative selection in *Streptococcus pneumoniae*. Appl Environ Microbiol. 2001; 67:5190–5196. [PubMed: 11679344]

Tottey S, Waldron KJ, Firbank SJ, Reale B, Bessant C, Sato K, Cheek TR, Gray J, Banfield MJ, Dennison C, Robinson NJ. Protein-folding location can regulate manganese-binding versus copper- or zinc-binding. Nature. 2008; 455:1138–1142. [PubMed: 18948958]

Treuner-Lange A, Ward MJ, Zusman DR. Pph1 from *Myxococcus xanthus* is a protein phosphatase involved in vegetative growth and development. Mol Microbiol. 2001; 40:126–140. [PubMed: 11298281]

Tsui HC, Mukherjee D, Ray VA, Sham LT, Feig AL, Winkler ME. Identification and characterization of noncoding small RNAs in *Streptococcus pneumoniae* serotype 2 strain D39. J Bacteriol. 2010; 192:264–279. [PubMed: 19854910]

Ulijasz AT, Andes DR, Glasner JD, Weisblum B. Regulation of iron transport in *Streptococcus pneumoniae* by RitR, an orphan response regulator. J Bacteriol. 2004; 186:8123–8136. [PubMed: 15547286]

Ulijasz AT, Falk SP, Weisblum B. Phosphorylation of the RitR DNA-binding domain by a Ser–Thr phosphokinase: implications for global gene regulation in the streptococci. Mol Microbiol. 2009; 71:382–390. [PubMed: 19040630]

Ulrych A, Holeckova N, Goldova J, Doubravova L, Benada O, Kofronova O, Halada P, Branny P. Characterization of pneumococcal Ser/Thr protein phosphatase phpP mutant and identification of a novel PhpP substrate, putative RNA binding protein Jag. BMC Microbiol. 2016; 16:247. [PubMed: 27776484]

van Opijnen T, Bodi KL, Camilli A. Tn-seq: high-throughput parallel sequencing for fitness and genetic interaction studies in microorganisms. Nat Methods. 2009; 6:767–772. [PubMed: 19767758]

Wehenkel A, Bellinzoni M, Schaeffer F, Villarino A, Alzari PM. Structural and binding studies of the three-metal center in two mycobacterial PPM Ser/Thr protein phosphatases. J Mol Biol. 2007; 374:890–898. [PubMed: 17961594]

Wu HJ, Seib KL, Srikhanta YN, Kidd SP, Edwards JL, Maguire TL, Grimmond SM, Apicella MA, McEwan AG, Jennings MP. PerR controls Mn-dependent resistance to oxidative stress in *Neisseria gonorrhoeae*. Mol Microbiol. 2006; 60:401–416. [PubMed: 16573689]

Yesilkaya H, Kadioglu A, Gingles N, Alexander JE, Mitchell TJ, Andrew PW. Role of manganese-containing superoxide dismutase in oxidative stress and virulence of *Streptococcus pneumoniae*. Infect Immun. 2000; 68:2819–2826. [PubMed: 10768978]

Zackular JP, Chazin WJ, Skaar EP. Nutritional Immunity: S100 Proteins at the Host-Pathogen Interface. J Biol Chem. 2015; 290:18991–18998. [PubMed: 26055713]

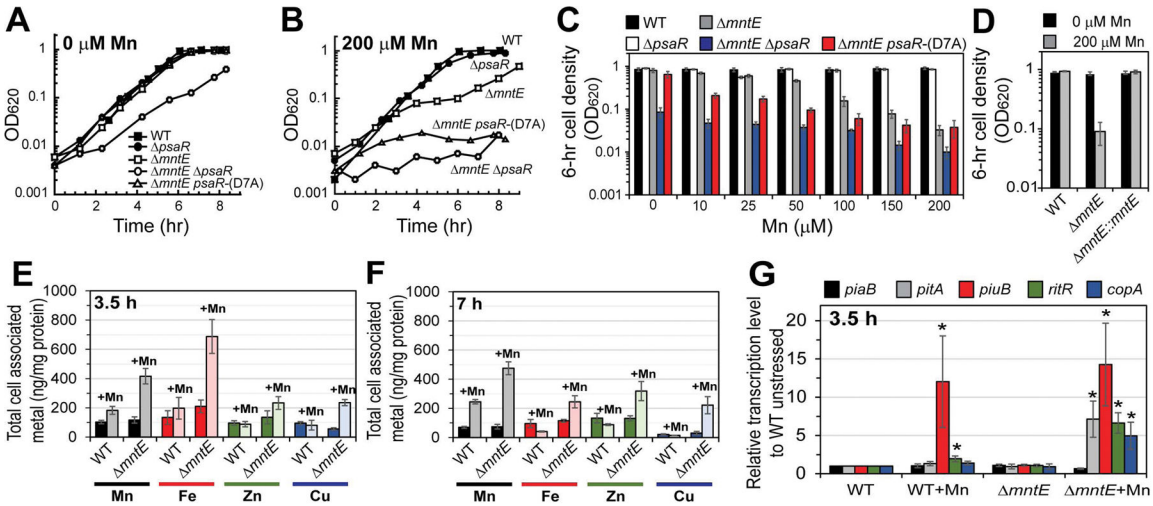

Figure 1. Manganese homeostasis is critical for cell growth

Exponentially growing cells were diluted into pre-warmed BHI broth containing increasing concentrations of Mn at time zero and allowed to proliferate. (**A**) BHI only, (**B**) BHI supplemented with 200 μM Mn, (**C**) growth yield after 6-h growth post inoculation in BHI supplemented with varying Mn concentrations, and (**D**) complementation of Δ*mntE* mutation in BHI with or without 200 μM Mn. Total cell-associated metal at 3.5 (**E**) or 7 h (**F**) from cells grown with 0 (*darker shade*) or 200 μM (*lighter shade*) Mn. (**G**) Relative transcript levels of RNA isolated from cells grown in BHI with or without 200 μM Mn for 3.5 h. *$P \leq 0.05$. Data shown are representative of at least three independent growth experiments for (**A, B**). The mean of at least three independent cultures ± SEM is shown for (**C–G**).

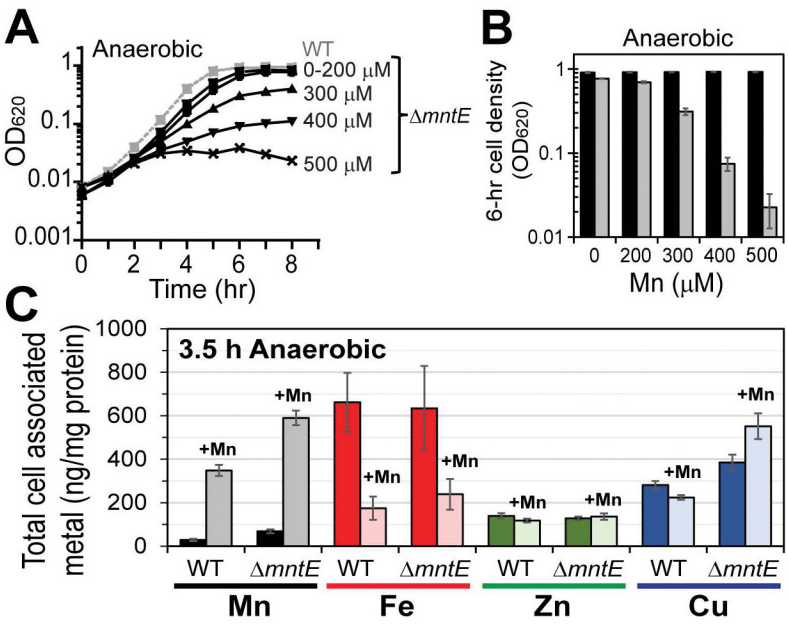

Figure 2. Anaerobically growing cells are sensitive to manganese toxicity

Anaerobic cultures were diluted into pre-warmed BHI broth with increasing concentration of Mn at time zero and allowed to proliferate anaerobically. (**A**) Growth over time. Representative WT growth with 0–500 μM Mn supplementation shown (*grey squares*, *dashed*). (**B**) Growth yield at 6 h for WT (*black*) and *mntE*-null mutants (*grey*). (**C**) Total cell-associated metal at 3.5 h from cells grown with 0 (*darker shade*) or 200 μM (*lighter shade*) Mn. The mean of at least three independent cultures ± SEM is shown. Note that Fe levels are dramatically reduced for both wild-type and Δ*mntE* strains to a similar level observed by aerobic non-stressed strains (see Fig. 1E) when grown anaerobically with excess Mn.

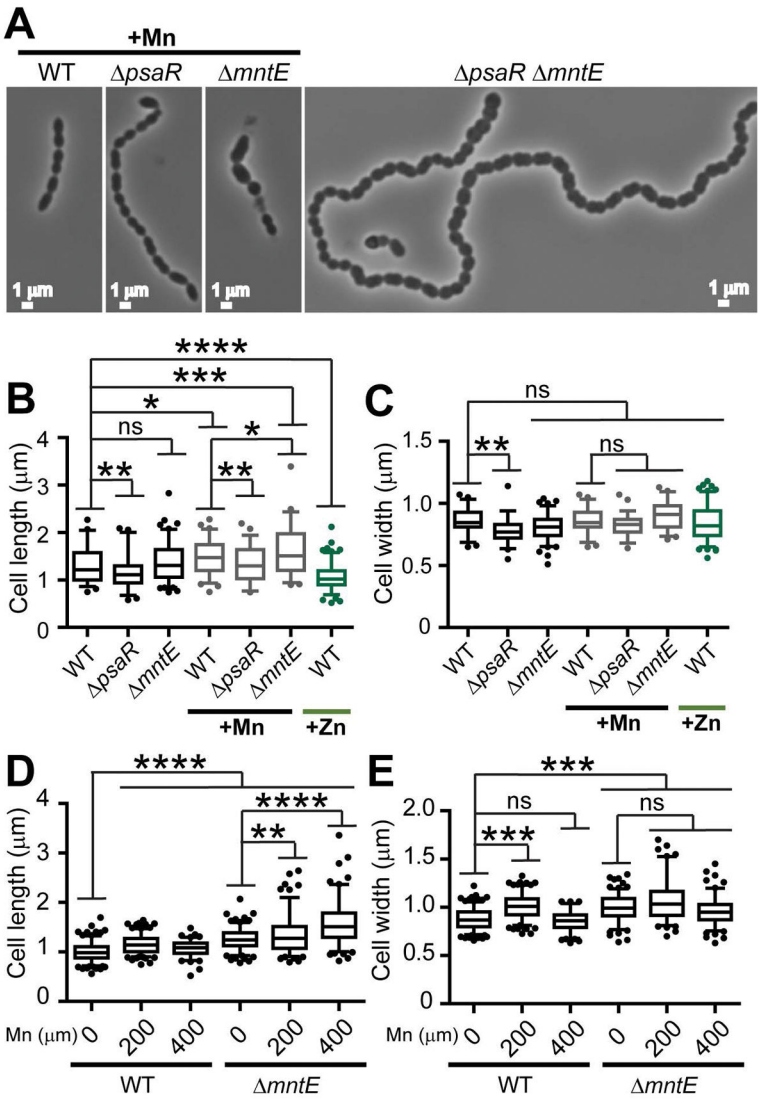

Figure 3. Cell division is disrupted by Mn-toxicity

(**A**) Representative morphology of cells grown in BHI supplemented with 200 μM Mn at 3.5 h post-inoculation. No Mn was added to the double Δ*psaR* Δ*mntE* mutant. Length (**B**) and width (**C**) measurements of cells grown with 0, 200 μM Mn, or 200 μM Zn. Length (**D**) and width (**E**) measurements of cells grown anaerobically with 0, 200, or 400 μM Mn. *$P \leq 0.10$; **$P \leq 0.05$; ***$P \leq 0.01$; ****$P \leq 0.001$; ns, not significant.

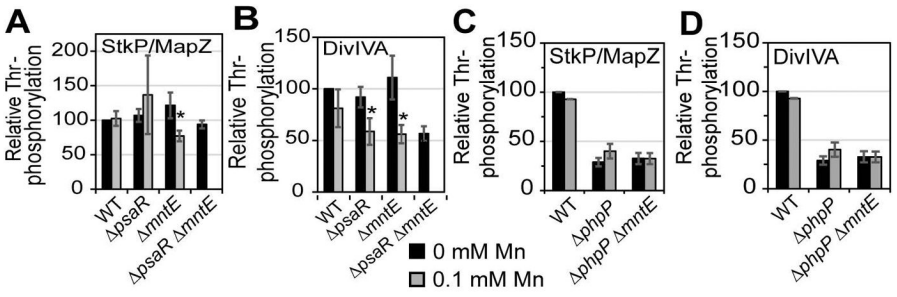

Figure 4. PhpP cell division target proteins are hypo-phosphorylated during Mn stress

Relative Thr-phosphorylation of StkP/MapZ (panels A, C) and DivIVA (panels B, D) by Western blot from different pneumococcal strains as indicated grown aerobically with 0 (*black*) or 100 μM (*grey*) Mn. Intensities are normalized to wild-type untreated cells and the mean is shown for at least four independent experiments ± SEM. *$P \leq 0.05$.

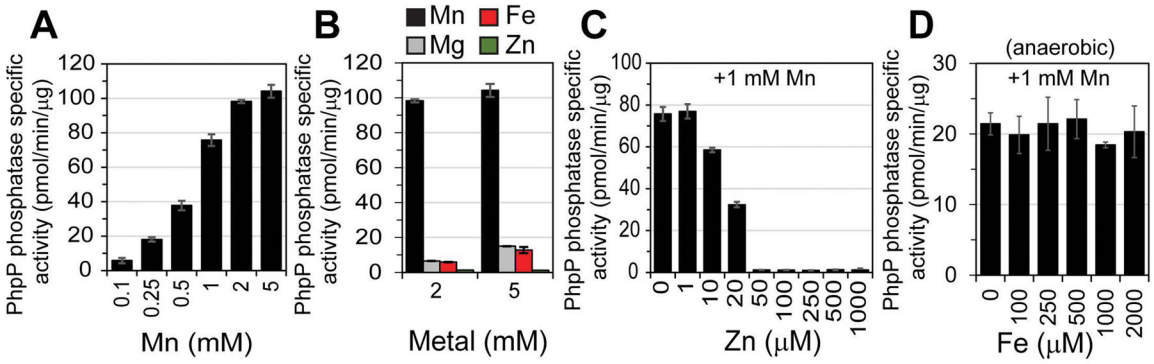

Figure 5. Mn:Zn ratio influences PhpP specific activity *in vitro*

(**A**) Activation of purified apo-PhpP with increasing concentrations of Mn(II). (**B**) Comparison of PhpP activation using different metal cations. (**C**) Titration of Zn(II) into a 1 mM Mn(II) reaction containing 730 nM apo-PhpP. (**D**) Anaerobic titration of Fe(II) into a 1 mM Mn(II) reaction containing apo-PhpP. Data shown represent the mean of three independent measurements ± SEM for all.

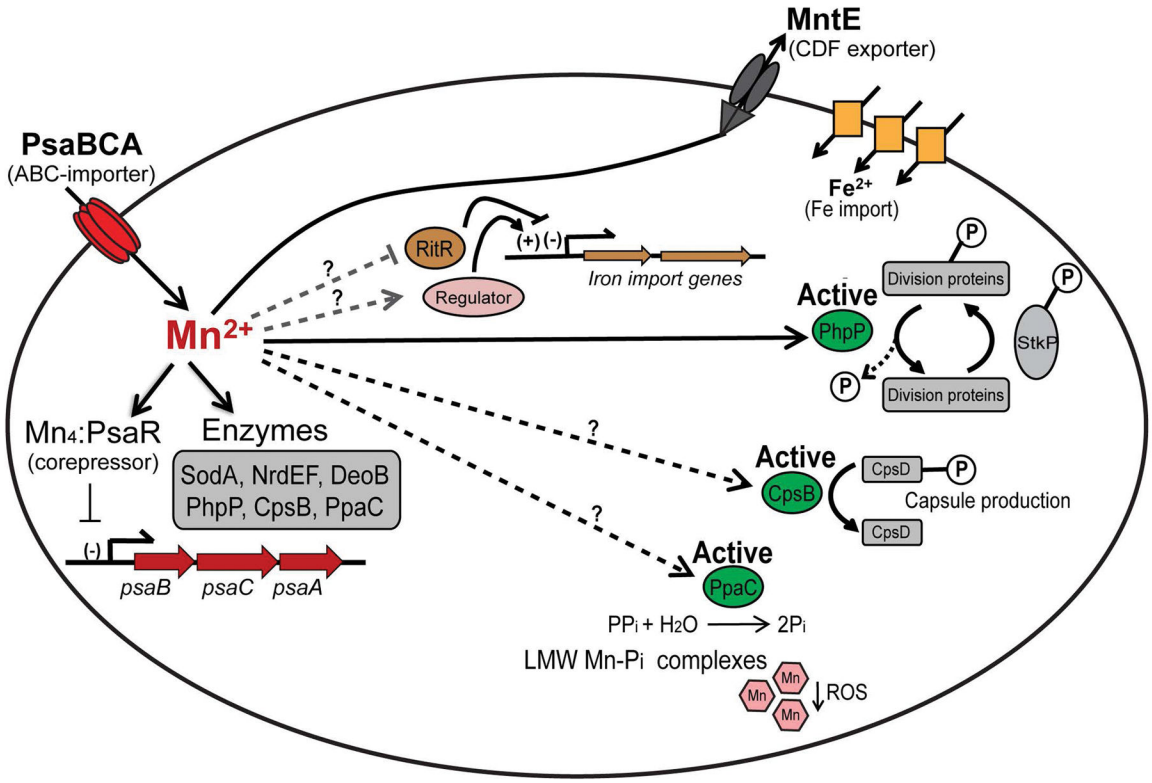

Figure 6. Overview of manganese metabolism in *S. pneumoniae*

Mn is imported into the cell by PsaBCA. Imported Mn is used to metallate a relatively small number of Mn-utilizing enzymes, including SodA, NrdEF, DeoB, PpcA, CpsB, and PhpP; see text for functional descriptions. During Mn-replete conditions Mn-bound PsaR represses transcription of *psaBCA*, thereby reducing Mn import. Excess Mn is effluxed from the cytoplasm by the constitutively expressed MntE exporter (Martin and Giedroc, 2016; Rosch *et al.*, 2009). Failure of MntE to properly export Mn results in accumulation of cell-associated Mn (see Fig. 2) and hyperactivation of Thr/Ser-phosphatase PhpP, which in turn leads to hyper-dephosphorylation of cell division proteins. Excess Mn may also inhibit the orphan response regulator, which leads to induction of expression of Fe import genes. Mn may also activate an, as yet, unidentified regulatory protein that is involved in regulating Fe homeostasis. In addition, Mn may regulate capsule biosynthesis via the Mn-dependent protein phosphatase-kinase pair, CpsB/CpsD, or help reduce reactive oxygen species via formation of low molecular weight (LMW) Mn-phosphate (P_i) complexes through activation of the Mn-dependent inorganic pyrophosphatase, PpaC.